Experimental Study of the Turbulent Boundary Layer on a Transport Wing in Subsonic Flow

Frank W. Spaid*
McDonnell Douglas Corporation, St. Louis, Missouri

The upper-surface boundary layer on a transport wing model was extensively surveyed with miniature yaw probes at a subsonic cruise condition. Significant variation in flow direction with distance from the surface was observed near the trailing edge, everywhere except at the wing root and tip. Values of streamwise displacement thickness, normalized by the local chord, were maximum at the highly loaded midsemispan stations. The data are intended to provide a test case for computational fluid dynamics code validation.

Nomenclature

b = wingspan
c = section chord
C_f = local skin-friction coefficient, τ/q_e
C_p = pressure coefficient, $(p - p_\infty)/q_\infty$
H = streamwise boundary-layer shape factor, δ_1^*/θ_{11}
M = Mach number
p = pressure
q = dynamic pressure, $(1/2)\rho u^2$
Re_c = Reynolds number based on chord
u = velocity magnitude, $u^2 = u_s^2 + w^2$
u_s = component of velocity parallel to boundary-layer-edge flow direction
u_τ = shear velocity, $\sqrt{\tau_w/\rho_w}$
w = component of velocity normal to boundary-layer-edge flow direction
x = coordinate measured parallel to freestream direction
y = spanwise coordinate
z = coordinate normal to wing mean reference plane
α = angle of attack with respect to model planform reference plane
β = yaw-plane flow direction angle measured with respect to u_∞, positive outboard
δ_1^* = streamwise displacement thickness, $\int_0^\infty [1 - (\rho u_s/\rho_e u_e)]\, dz$
δ_2^* = crossflow displacement thickness, $-\int_0^\delta (\rho w/\rho_e u_e)\, dz$
η = normalized semispan, $2y/b$
θ_{11} = streamwise displacement thickness, $\int_0^\delta (\rho u_s/\rho_e u_e)(1 - u_s/u_e)\, dz$
ν = kinematic viscosity
ρ = density
τ = shear stress determined from velocity magnitude profiles

Subscripts
e = conditions at edge of boundary layer
w = conditions at surface
∞ = freestream conditions

Introduction

RECENT progress in the development of methods for computation of wing flowfields has led to a need for experimental data that can be used to evaluate the accuracy and range of applicability of the computed predictions.[1] Low-speed experiments in flows related to the flow about a swept wing are reported by van den Berg et al.[2] and Seetharam et al.[3] The present study describes efforts to provide an experimental description of the boundary layer on most of the upper surface of a typical transport wing in subsonic flow. Data from this investigation are also presented in Refs. 4–7. This study is part of a cooperative program among McDonnell Douglas Research Laboratories, Douglas Aircraft Company, and the NASA Ames Research Center (ARC).

Facilities and Equipment

The experiments were conducted in the NASA-ARC, 14-Ft Transonic Wind Tunnel. This facility is a continuous-flow tunnel; the stagnation pressure is atmospheric, and the stagnation temperature is controlled by exchanging air with the surrounding atmosphere. The semispan model wing, fuselage, and probe traversing assembly installed in the test section are shown in Fig. 1. The test-section walls are slotted, but steel plates were used to cover the floor slots during this test.

The wing model was obtained from Douglas Aircraft Company. It has a 1.113-m semispan and a 0.359-m mean aerodynamic chord. Figure 2 is a plan view of the model and includes some geometric properties of the wing. The wing is instrumented with 378 static-pressure orifices located at nine spanwise stations.

The fuselage is one-half of a body of revolution, under which a 3.18-cm-thick uniform section was added. An auxiliary wing with a probe traversing unit is attached to the fuselage downstream of the primary wing. The undisturbed tunnel-wall boundary layer is approximately 18–20 cm thick at the model station,[8] the displacement thickness is approximately 3.2 cm, and the ratio of the undisturbed velocity at the height of the wing root (16.5 cm above the tunnel floor) to the freestream velocity u_∞ is approximately 0.97. The model is small relative to the test section; the blockage ratio is 0.45%, and the ratio of semispan to tunnel height is 0.26.

Good technique in obtaining three-dimensional, boundary-layer data typically includes the use of probes attached to the surface near the measuring station and alignment of the tips with the local flow direction by a nulling technique. The high cost of operating a large transonic wind tunnel and the limited availability of such facilities for research investigations precluded such a time-consuming approach. It was decided that a traversing unit allowing remote streamwise positioning and flow-direction measurements using fixed-position probe tips would be required to complete the study in approximately one month of tunnel occupancy.

The model and traversing mechanism used in this study are shown schematically in Figs. 2 and 3. An auxiliary wing with a traversing unit is attached to the fuselage downstream of the primary wing. The constant-chord auxiliary wing is swept 20 deg and lies approximately in the mean chord plane of the primary wing. The auxiliary wing is mounted at −1.5 deg

Received Dec. 24, 1988; revision received Dec. 27, 1989.

*Chief Scientist, McDonnell Douglas Research Laboratories. Associate Fellow AIAA.

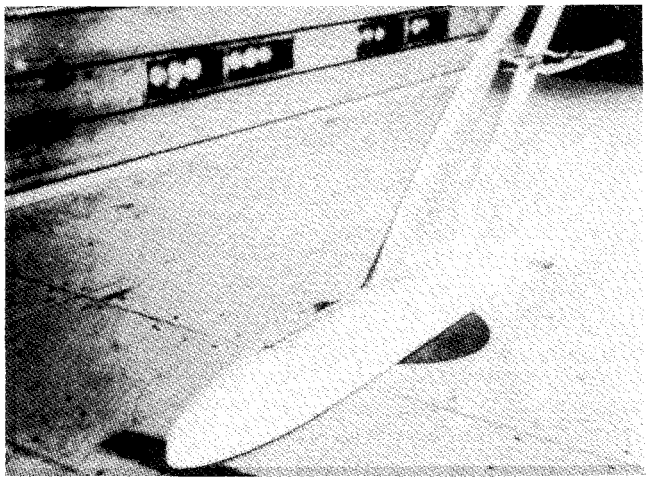

Fig. 1 Transport model with traversing unit in NASA-ARC 14-Ft transonic wind tunnel.

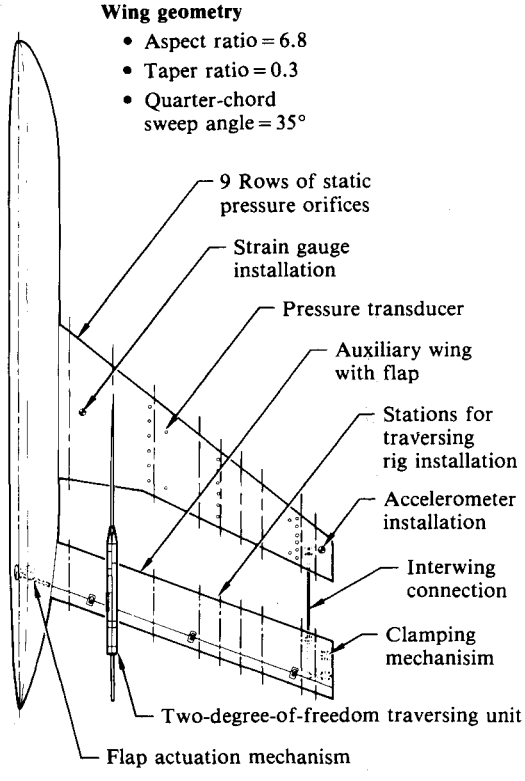

Fig. 2 Wing, fuselage, and boundary-layer traversing unit.

incidence relative to the fuselage centerline because panel-method calculations indicated that this alignment would minimize interference in the flow about the primary wing at subsonic conditions. The auxiliary wing has a remotely actuated trailing-edge flap for minimizing interference at test conditions other than the primary subsonic condition. The flap chord is 20% of the auxiliary wing chord. A strut connecting the two wing tips, also shown in Fig. 2, is intended to minimize their relative unsteady motion. The strut is pinned to the primary wing and to the auxiliary wing near the leading edge. A remotely actuated pneumatic clamp, designed to minimize relative vibration between the two wings, is located near the auxiliary-wing trailing edge.

A two-degree-of-freedom traversing unit was installed in succession at the nine spanwise stations on the auxiliary wing, thus allowing boundary-layer profiles to be obtained along each row of static-pressure orifices. The principal features of

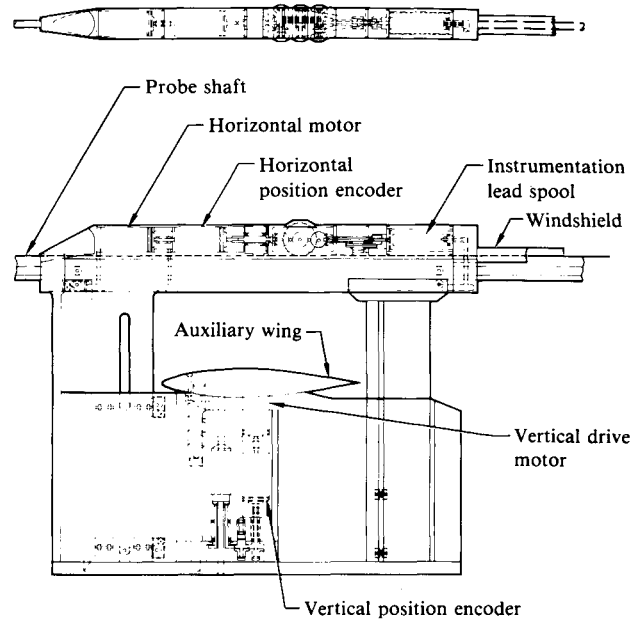

Fig. 3 Details of traversing unit.

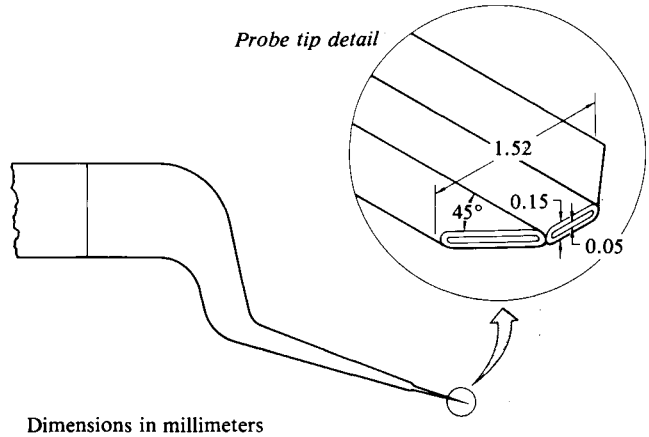

Fig. 4 Probe geometry.

the traversing unit are shown in Fig. 3. The design of this device was influenced by compromises between flow interference and rigidity. Probe tips are attached to a rectangular probe shaft that moves though a housing containing the horizontal-drive stepper motor, horizontal-position encoder, and instrumentation-lead rewind spool. Maximum streamwise travel is 48 cm with a resolution of 0.0866 mm per encoder pulse. The design of this traversing unit and the auxiliary wing was a compromise between rigidity and flowfield interference.

Motion and readout in the direction normal to the wing are provided by a similar motor-encoder assembly installed in the airfoil-shaped strut located below the auxiliary wing. The range of travel normal to the wing is 7.6 cm; this motion is accommodated by a coil of instrumentation leads within the strut. Position resolution is 0.0052 mm per encoder pulse. Play and backlash are eliminated in both directions by spring-loaded bearings and antibacklash gearing.

Probe tips are small, flattened, three-orifice yaw probes (see Fig. 4), similar to those described by Dudzinski and Krause.[9] Calibration of these probes allowed determination of the flow speed and its direction in the plane of the wing. The probe tips were electrically insulated from the probe shaft to allow the wing surface to be located by an electrical contact during a test.

A number of profiles at inboard stations near the trailing edge were obtained outside of the pitch angle range of ± 10

deg, for which errors in measured stagnation pressure are negligible. Posttest calibration data appropriate to the actual pitch misalignment range were used to reduce the data obtained with probes 2 and 3. Errors in measured yaw angle caused by pitch misalignment were small, and therefore no corrections to yaw angle for effects of pitch misalignment were made. Boundary-layer-edge values of stagnation pressure obtained from the data from probes 2 and 3 agreed with the freestream value to within 0.5% for 85% of the profiles. Typical errors in data obtained with the first probe are larger, but the satisfactory agreement between data obtained with the first probe and data obtained with the second and third indicates that effects of pitch misalignment in the data from the first probe are minor.

Probe data and test-section conditions were recorded with the aid of a control unit and a microcomputer and stored on flexible disks. A boundary-layer survey was performed by a preprogrammed sequence of probe motions and data acquisition cycles. Primary-wing static pressures and test-section conditions were acquired by the wind-tunnel data system.

Boundary-layer transition trips were applied on both upper and lower surfaces at 6% local chord, following the recommendations of Braslow et al.[10] The roughness elements were spherical glass beads having a nominal diameter of 0.13 mm. This size corresponds to 1.5 k to 2 k, where k is the minimum-size element that will cause transition to occur at the trip.

Results and Discussion

Data obtained from this investigation are summarized in the following sections. A more detailed description of the experiment and presentation of the results are included in Ref. 7.

Static Pressures and Tuft Flow Visualization

Upper-surface, boundary-layer data were obtained at the following test conditions: Mach number, $M_\infty = 0.50$; Reynolds number based on mean aerodynamic chord, $Re_c = 3.4 \times 10^6$; angle of attack, $\alpha = 6$ deg; and wing-lift coefficient, $C_L = 0.583$. Sublimation flow visualization data obtained at this test condition indicated that transition occurred forward of the boundary-layer trip at spanwise locations inboard of 90% semispan; transition occurred at the trip outboard of this station.

Static-pressure distributions obtained at all nine spanwise pressure-orifice stations corresponding to the test condition for which boundary-layer data were obtained are shown superimposed on the wing planform in Fig. 5. The suction peaks in these pressure distributions are strongest at the midsemispan stations; the peaks decrease near the tip as a result of the wing twist. Interference of the auxiliary wing and traversing unit on the flow about the primary wing, as indicated by static-pressure data, was no greater than differences associated with run-to-run repeatability for this test condition.

Prior to each boundary-layer survey, a set of wing static-pressure data was obtained with the probe near the surface in position for the survey. Static-pressure distributions obtained upstream of the probe location are superimposed in Fig. 6 on the corresponding distributions obtained with the probe retracted. The probe-tip interference effects are similar to, but smaller than, the effects observed in the airfoil experiments reported in Ref. 11. Where interference effects are present, they usually take the form of an additional adverse static-pressure gradient. Interference associated with the probe tip was negligible when the probe tip was aft of midchord, and interference at forward survey stations was minor.

Results of an attempt to determine the effects of similar static-pressure perturbations on boundary-layer properties are summarized n Ref. 11, where it is tentatively concluded that these effects are small if the noninterference C_p is used in computing velocities from pitot-pressure data.

A fluorescent minituft, flow-visualization photograph corresponding to the test conditions shown in Fig. 5 is presented in Fig. 7. The tufts are 0.05-mm-diam monofilament nylon,

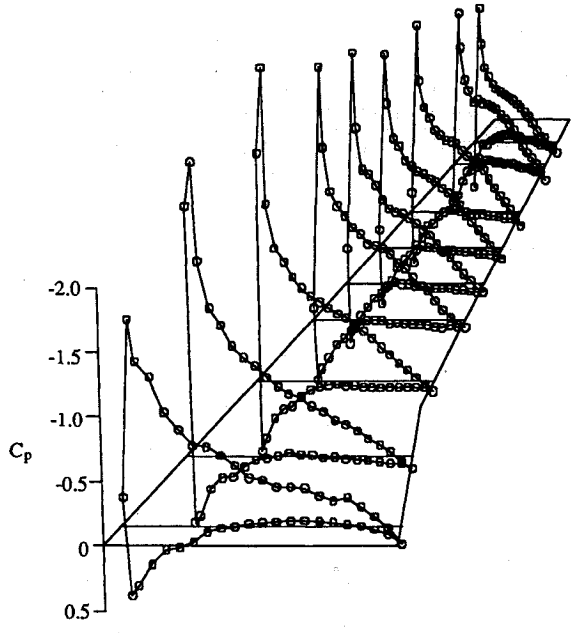

Fig. 5 Wing static-pressure distribution, subsonic test condition, $M_\infty = 0.50$, $\alpha = 6$ deg.

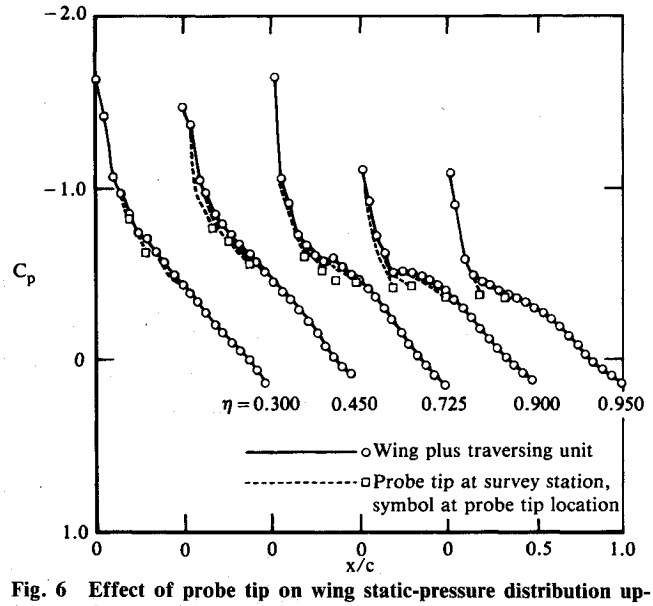

Fig. 6 Effect of probe tip on wing static-pressure distribution upstream of survey station, $M_\infty = 0.5$, $\alpha = 6$ deg.

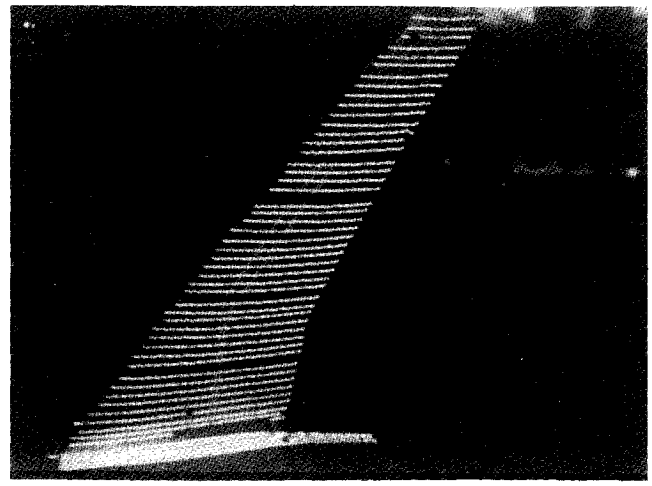

Fig. 7 Flourescent minituft flow visualization, $M_\infty = 0.5$, $\alpha = 6$ deg.

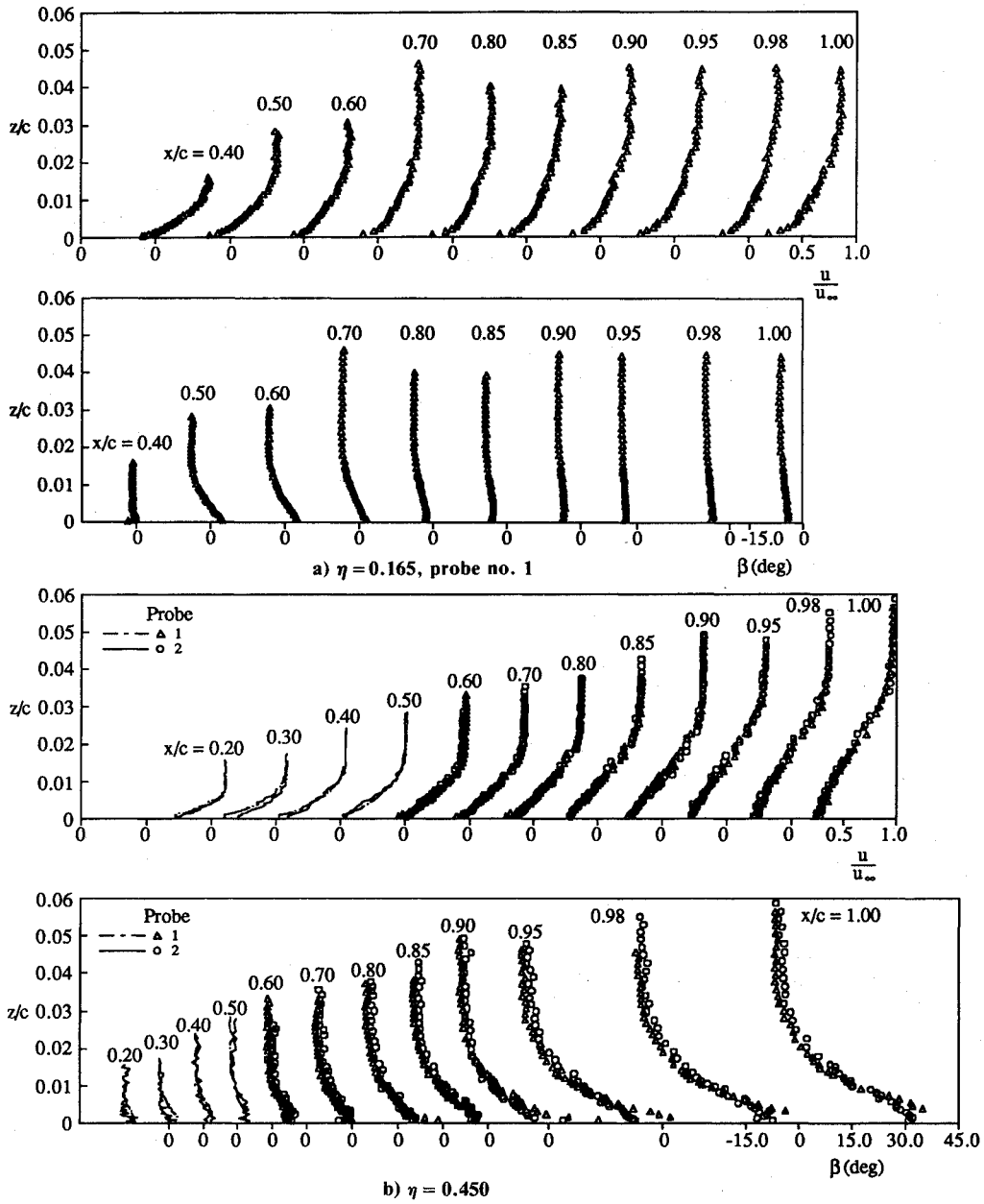

Fig. 8 Boundary-layer profiles.

dyed with a fluorescent dye and cemented to the model surface. The rows of tufts lie in planes parallel to the plane of symmetry of the model. The tuft pattern was photographed during a run by use of an ultraviolet flash. The minituft technique was developed by Crowder.[12] The region of missing tufts in the central portion of the planform in Fig. 7 was caused by flow unsteadiness before this photograph was taken; the wing and tufts had been subjected to severe test conditions, including higher Mach numbers and angles of attack, which were associated with extensive regions of flow separation on the central portion of the wing.

The flow at the wing root, as indicated by the tufts, is essentially unyawed. Deviation of the tufts from the streamwise direction is minor, except near the trailing edge, where outboard flow is indicated. The two rows of tufts nearest the tip show significant differences. The row nearest the tip shows the inboard flow forward and outboard flow aft, but the next row inboard does not show an outboard component of flow near the trailing edge.

Boundary-Layer Profiles

Velocity magnitude and flow-direction profiles are presented in Fig. 8. The ordinate z/c is the distance from the surface normalized by the local chord, and the velocity magnitude u is normalized by the freestream velocity. The flow inclination angle β is defined relative to the freestream flow direction, and positive values of β correspond to outboard flow. The use of the freestream direction as the reference for β allows both the variation in flow direction both through the boundary layer and along the chord to be presented in a single plot. Data obtained nearest the wing root $\eta = 0.165$ are included in Fig. 8a. The side of the fuselage is roughly planar above the wing, except for a small fillet at the wing-fuselage intersection, and is located at $\eta = 0.127$, 4.2 cm inboard of this spanwise survey station. The velocity magnitude profiles are moderately full and show some scatter resulting from flow unsteadiness. The direction profiles show nearly streamwise, collinear flow in the aft region with moderate outboard inclination at midchord near the surface.

The data of Fig. 8b at $\eta = 0.450$ are qualitatively different from the data obtained at the root station and are typical of the midsemispan stations. The velocity magnitude profiles at $\eta = 0.450$ show greater boundary-layer growth relative to the root station, and the flow-direction profiles show greater three dimensionality. The flow is inboard and nearly collinear at the forward stations. The magnitude of the edge inclination de-

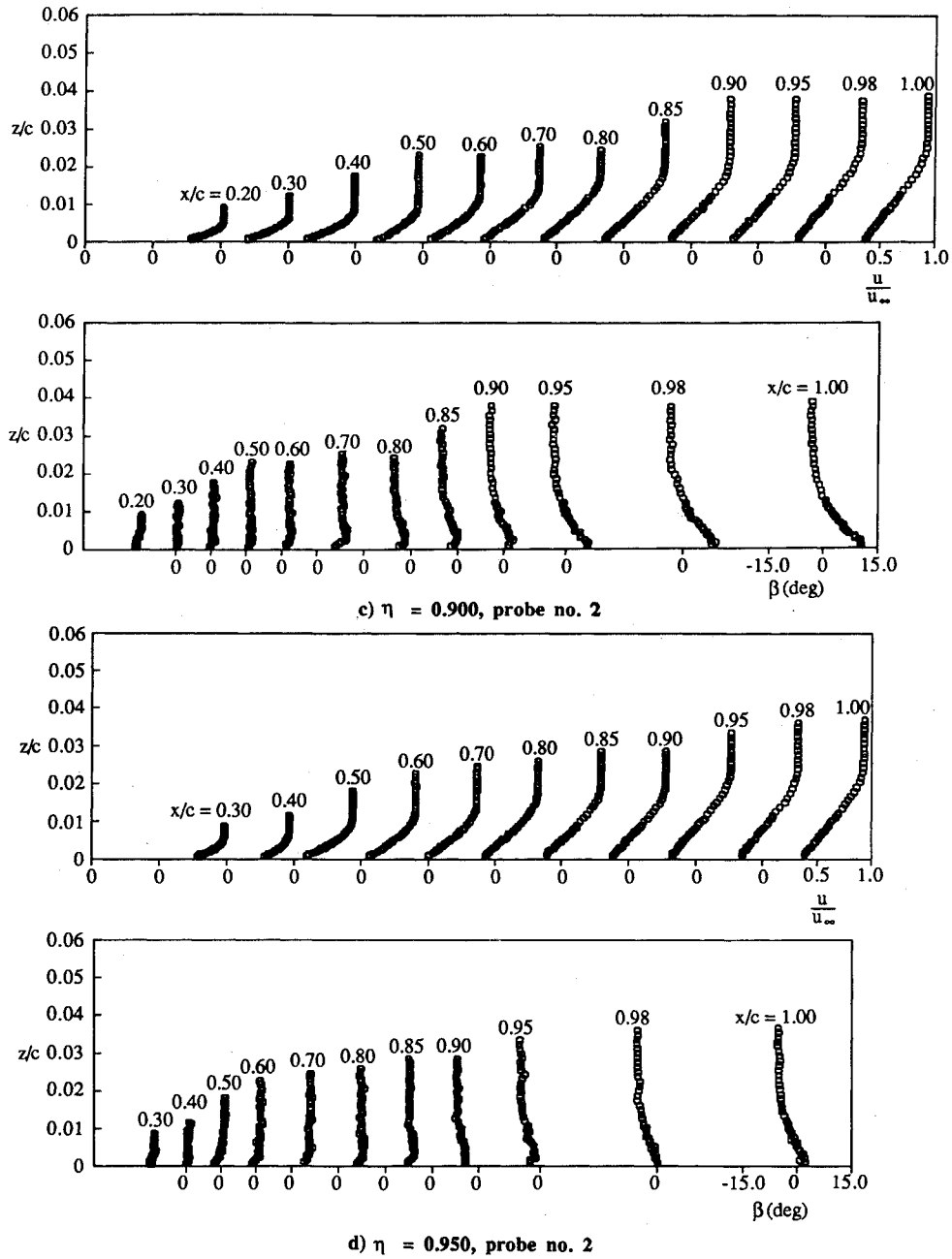

c) η = 0.900, probe no. 2

d) η = 0.950, probe no. 2

Fig. 8 Boundary-layer profiles (continued).

creases with increasing x/c, becoming nearly aligned with the freestream direction near the trailing edge. Profiles at the aft chordwise stations show the flow direction changing from slightly inboard at the edge to outboard near the surface—a trend that becomes more pronounced as the trailing edge is approached. Velocity magnitude and flow-direction data obtained with two different probes at the same chordwise station are in good agreement with each other.

The qualitative characteristics of the boundary-layer velocity magnitude and flow-direction profiles obtained at $\eta = 0.300$, 0.575, 0.650, and 0.725, are similar to the characteristics of the profiles obtained at $\eta = 0.450$. The influence of the wing twist and the associated reduction in section lift coefficient with increasing spanwise station near the tip are evident in the data obtained at the outboard stations $\eta = 0.900$ and 0.950, Figs. 8c–8d. The variation of flow direction with chordwise location at the boundary-layer edge is qualitatively the same as at the inboard stations. Profiles at forward chordwise locations are approximately collinear. Both the growth in boundary-layer thickness with increasing chordwise distance and the variation in flow direction through the boundary layer near the trailing edge decrease abruptly as the tip is approached.

For two-dimensional turbulent boundary layers, a generally accepted near-wall similarity law is

$$\frac{u}{u_\tau} = \frac{1}{0.41} \ell n \left(\frac{z u_\tau}{\nu} \right) + 5 \tag{1}$$

Pierce et al.[13] concluded that the magnitude of the wall shear stress could be determined with the aid of Eq. (1) by the Clauser chart technique[14] to within 5–10% if data in the range $10 \le z^+ \le 100$ ($z^+ = z u_\tau / \nu_w$) were used. This conclusion was limited to monotonically skewed boundary layers with an approximate maximum of 15–20 deg of skew.

Figure 9 illustrates the method by which the Clauser chart technique was applied to the present data. Velocity magnitudes obtained at $\eta = 0.165$ and 0.950 are plotted in semilogarithmic coordinates. In these coordinates, Eq. (1) represents a family of straight lines with the skin-friction coefficient as a parameter. Since the straight lines in Fig. 9 represent the range $10 \le z^+ \le 1000$, it is apparent that the sublayer and the inner

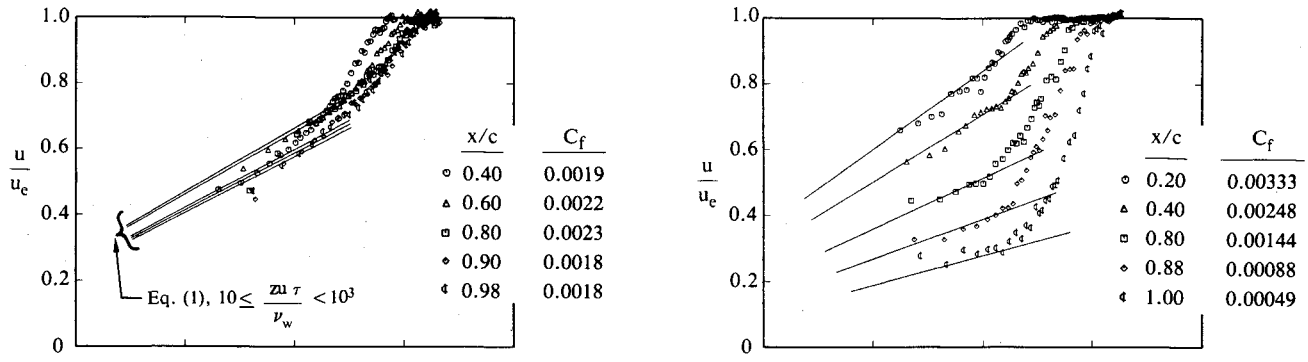

Fig. 9 Velocity-magnitude profiles in semilog coordinates.

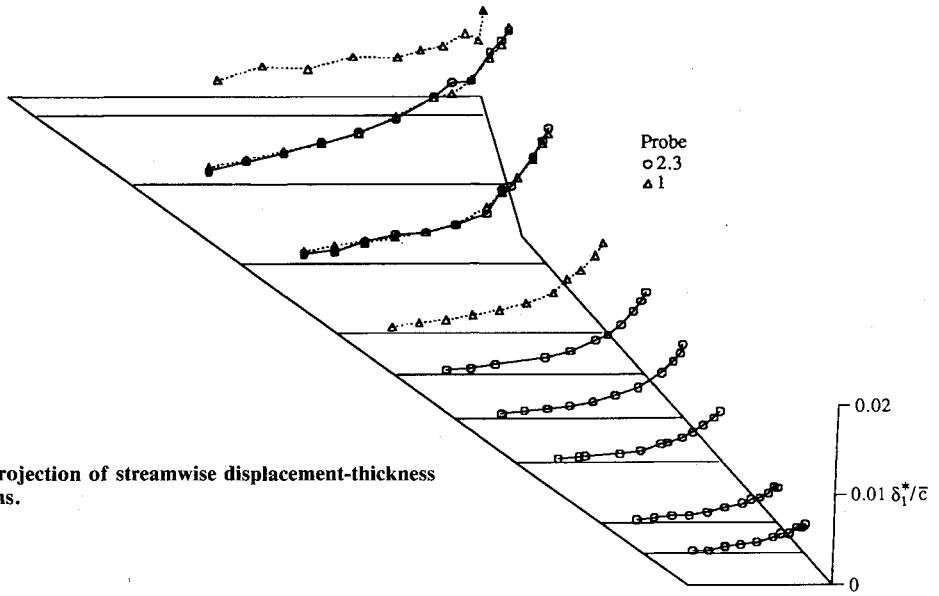

Fig. 10 Projection of streamwise displacement-thickness distributions.

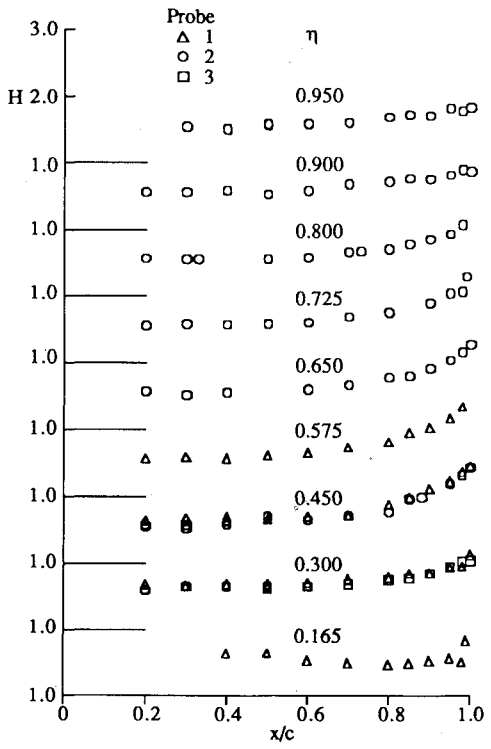

Fig. 11 Shape factor distributions.

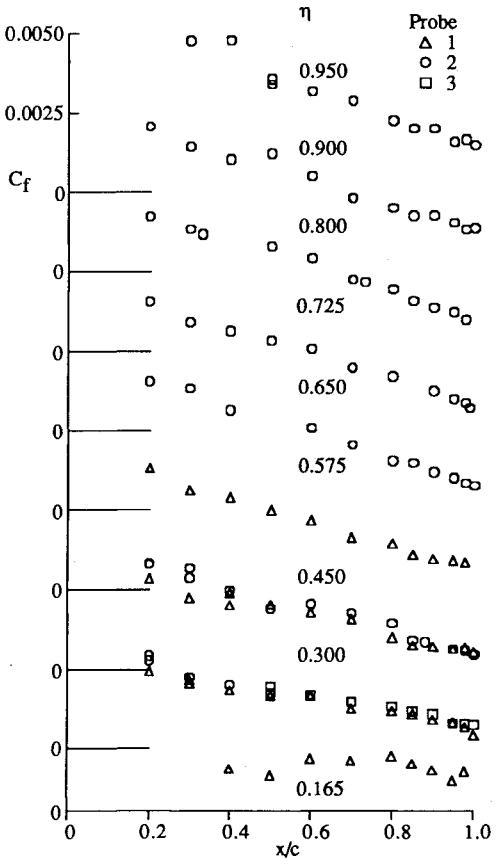

Fig. 12 Skin-friction distributions.

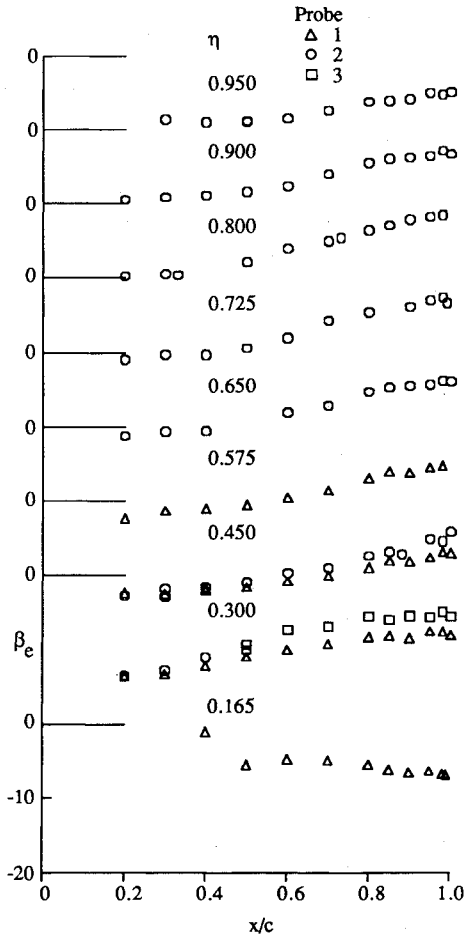

Fig. 13 Distributions of yaw-plane flow direction at the boundary-layer edge.

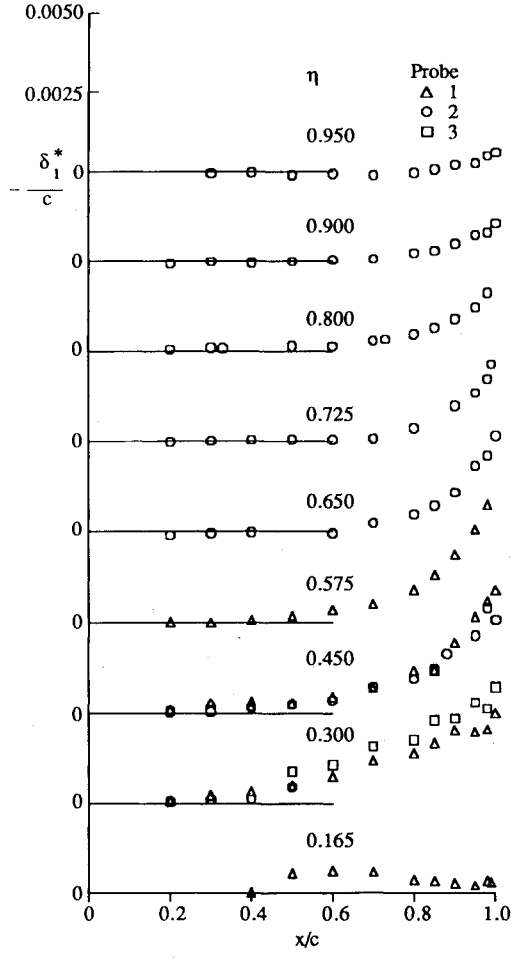

Fig. 14 Crossflow displacement-thickness distributions.

portion of the logarithmic region are not resolved in these data. For this reason, most of the velocity magnitude profiles do not appear to approach zero with decreasing distance from the wall. In some cases, where a well-defined logarithmic region exists, the data obtained nearest the surface lie above the law of the wall. This trend has been observed in airfoil boundary-layer measurements and is believed to be a surface proximity effect, probably also related to relative motion of the model and traversing unit. Note that the maximum skewing angles corresponding to many of the profiles of this investigation exceed the range of applicability of this method for estimating skin friction. Near the trailing edge at the midsemispan stations, the difference in β between the boundary-layer edge and the surface sometimes exceeds 35 deg. For the more highly skewed profiles, it is likely that values of C_f estimated by this method represent the correct order of magnitude.

The behavior of the boundary-layer profiles obtained at the wing root, $\eta = 0.165$, is qualitatively different from that of the profiles at the other spanwise stations. Although these profiles do exhibit a logarithmic region near the surface, the slope is greater than that given by Eq. (1).

Integral Properties, Skin Friction, and Edge-Flow-Angle Data

Values of streamwise displacement thickness δ_1^*, for all of the profiles obtained at the subsonic test condition, are presented in Fig. 10, normalized by the mean aerodynamic chord. The streamwise and crossflow displacement thicknesses δ_1^* and δ_2^* are defined in the Nomenclature section. Agreement between data obtained at the same location with different probes is generally good. The increase in δ_1^* with x/c near the trailing edge is moderate at the root station, but the larger values of lift coefficient in the midsemispan region result in increased chordwise growth of δ_1^* with increasing x/c. This trend reverses near the tip as a result of reduced tip loading. The trailing-edge streamwise displacement thickness normalized by the local chord varies by nearly a factor of two from midsemispan to the tip. Values of δ_1^* are more scattered near the tip than similar data obtained farther inboard, probably because of vibration since the boundary layer was thinnest at the tip where the relative motion was greatest.

Values of streamwise shape factor H are presented in Fig. 11. These data show the expected increase near the trailing edge at midsemispan and more nearly constant values at the root and tip.

Values of skin friction obtained from the Clauser charts are presented in Fig. 12. The data show little variation at the root and monotonically decreasing values of C_f with increasing x/c at the other spanwise stations. Data obtained with different probes at the same location are in good agreement. The trends in the skin-friction data are consistent with trends observed in the δ_1^* and H plots.

Flow-direction measurements at the boundary-layer edge are presented in Fig. 13. Although all the previous comparisons show significant differences between trends observed at the wing root and at the other spanwise stations, the flow direction results are the most dramatic in this respect. The need for additional data in the transition region between the root and the midsemispan stations is apparent.

The crossflow displacement thickness δ_2^* is probably the most clear-cut indicator of three dimensionality. Distributions of crossflow displacement thickness are presented in Fig. 14. The trends in these data are consistent with the velocity magnitude and flow-direction profiles of Fig. 8; the most significant crossflow effects are present at midsemispan, aft of midchord.

Concluding Remarks

Boundary-layer survey data were obtained over most of the upper surface of a transport wing model at a subsonic test condition. The data were obtained with miniature three-orifice yaw probes that allowed determination of the flow speed and its direction in the plane of the wing. Surveys were obtained at nine spanwise stations and 10–12 chordwise stations at each spanwise station, from 20% chord to the trailing edge. Detailed velocity magnitude and yaw-plane flow direction angle data are presented here for four spanwise stations. Significant variation in flow direction with distance from the surface was observed near the trailing edge except at the wing root and tip. Values of skin friction were estimated from velocity magnitude profiles by the Clauser chart technique. The profile data were integrated to obtain streamwise and crossflow displacement-thickness distributions and streamwise shape-factor distributions. In addition to the boundary-layer data, surface static-pressure distributions and fluorescent minituft flow-visualization photographs were also obtained.

Compromises in the design of the data-acquisition equipment related to flow interference and rigidity were necessary to permit acquisition of an extensive set of data in a reasonable period of wind-tunnel occupancy. The influence of the traversing unit on the wing static-pressure distributions was negligible. The internal consistency of the data, including generally good repeatability, indicates that the data should provide useful test cases for three-dimensional, turbulent, boundary-layer computation methods.

Acknowledgments

This research was conducted under the McDonnell Douglas Independent Research and Development program in cooperation with the NASA Ames Research Center. The authors express their appreciation for the contributions and assistance of N. L. Vignati (McDonnell Douglas Research Labs.), F. T. Lynch, P. Henne, D. H. Newhart, (Douglas Aircraft Co.) R. M. Hicks, G. T. Chapman, L. L. Presley (NASA-ARC), and many others at McDonnell Douglas Corp., NASA-ARC, Sverdrup Technology, Inc., and Centro Corporation of Dayton, Ohio.

References

[1]Nixon, D., (ed.), *Transonic Aerodynamics: Progress in Astronautics and Aeronautics*, Vol. 81, AIAA, New York, 1982.

[2]van den Berg, B., Elsenaar, A., Lindhout, J. P. F., and Wesseling, P., "Measurements in an Incompressible Three-Dimensional Turbulent Boundary Layer Under Infinite Swept-Wing Conditions, and Comparison with Theory," *Journal of Fluid Mechanics*, Vol. 70, Pt. 1, Jan. 1975, pp. 127–148.

[3]Seetharam, H. C., Pfeiffer, N. J., Ohmura, M., and McLean, J. D., "Experimental and Theoretical Studies of Three-Dimensional Turbulent Boundary Layers on an Empennage of a Typical Transport Airplane," *Proceedings of the 13th Congress of ICAS*, AIAA, New York, 1982, pp. 784–795.

[4]Spaid, F. W., and Roos, F. W., "An Experimental Study of the Turbulent Boundary Layer on a Transport Wing in Transonic Flow," AIAA Paper 83-1687, July 1983.

[5]Spaid, F. W., "Transonic Airfoil and Wing Flowfield Measurements," AIAA Paper 84-0100, Jan. 1984.

[6]Spaid, F. W., "Comparisons Among Measured and Computed Boundary-Layer Properties on a Transport Wing," AIAA Paper 87-2555, Aug. 1987.

[7]Spaid, F. W., Roos, F. W., and Hicks, R. M., "An Experimental Study of the Turbulent Boundary Layer on a Transport Wing in Subsonic and Transonic Flow," NASA TM-102206, June 1990.

[8]Haney, H. P., Waggoner, E. G., and Ballhaus, W. F., "Computational Transonic Wing Optimization and Wind Tunnel Test of a Semi-Span Wing Model," AIAA Paper 78-102, Jan. 1978.

[9]Dudzinski, T. J., and Krause, L. N., "Flow-Direction Measurement with Fixed-Position Probes," NASA TM-X-1904, 1969.

[10]Braslow, A. L., Hicks, R. M., and Harris, R. V., Jr., "Use of Grit-Type Boundary-Layer-Transition Trips on Wind-Tunnel Models," NASA TN-D-3579, 1966.

[11]Spaid, F. W., and Stivers, L. S., Jr., "Supercritical Airfoil Boundary Layer Measurements," AIAA Paper 79-1501, July 1979.

[12]Crowder, J. P., "Fluorescent Mini-Tufts for Non-Intrusive Flow Visualization," McDonnell Douglas Corp., Long Beach, CA, MDC J7374, Feb. 1977.

[13]Pierce, F. J., McAllister, J. E., and Tennant, M. H., "Near-Wall Similarity in Three-Dimensional Turbulent Boundary Layers, Part II: Pressure-Driven Flow Results," *Three-Dimensional Turbulent Shear Flows*, The American Society of Mechanical Engineers, New York, 1982, pp. 96–103; see also *Journal of Aircraft*, Vol. 17, Aug. 1980, pp. 567–575.

[14]Clauser, F. H., "Turbulent Boundary Layers in Adverse Pressure Gradients," *Journal of Aeronautical Science*, Vol. 21, Feb. 1954, pp. 91–108.